Available online at www.sciencedirect.com

ScienceDirect

www.elsevier.com/locate/jes

JES JOURNAL OF ENVIRONMENTAL SCIENCES

www.jesc.ac.cn

Research Article

Mechanism of extracellular electron transport and reactive oxygen mediated Sb(III) oxidation by *Klebsiella aerogenes* HC10

Qun Rong [1,2], *Chaolan Zhang* [1,*], *Caiyuan Ling* [1], *Dingtian Lu* [1], *Linjiang Jiang* [1]

[1] *College of Resources, Environment and Materials Guangxi University, Nanning 530004, China*
[2] *School of Environment and Life Science, Nanning Normal University, Nanning 530001, China*

ARTICLE INFO

Article history:
Received 9 July 2023
Revised 11 September 2023
Accepted 12 September 2023
Available online 19 September 2023

Keywords:
Antimonite oxidation
Active oxygen
Free radical
Electron transfer
AQDS

ABSTRACT

Microbial oxidation and the mechanism of Sb(III) are key governing elements in biogeochemical cycling. A novel Sb oxidizing bacterium, *Klebsiella aerogenes* HC10, was attracted early and revealed that extracellular metabolites were the main fractions driving Sb oxidation. However, linkages between the extracellular metabolite driven Sb oxidation process and mechanism remain elusive. Here, model phenolic and quinone compounds, i.e., anthraquinone-2,6-disulfonate (AQDS) and hydroquinone (HYD), representing extracellular oxidants secreted by *K. aerogenes* HC10, were chosen to further study the Sb(III) oxidation mechanism. N_2 purging and free radical quenching showed that oxygen-induced oxidation accounted for 36.78% of Sb(III) in the metabolite reaction system, while hydroxyl free radicals (·OH) accounted for 15.52%. ·OH and H_2O_2 are the main driving factors for Sb oxidation. Radical quenching, methanol purification and electron paramagnetic resonance (EPR) analysis revealed that ·OH, superoxide radical ($O_2^{\bullet-}$) and semiquinone ($SQ^{-\bullet}$) were reactive intermediates of the phenolic induced oxidation process. Phenolic-induced ROS are one of the main oxidants in metabolites. Cyclic voltammetry (CV) showed that electron transfer of quinone also mediated Sb(III) oxidation. Part of Sb(V) was scavenged by the formation of the secondary Sb(V)-bearing mineral mopungite [$NaSb(OH)_6$] in the incubation system. Our study demonstrates the microbial role of oxidation detoxification and mineralization of Sb and provides scientific references for the biochemical remediation of Sb-contaminated soil.

Introduction

Antimony is a redox-active metal, and its toxicity and bioavailability vary with its chemical speciation. The toxicity of antimonite [Sb(III)] is higher than that of antimonate [Sb(V)] (Bolan et al., 2022). Antimony redox is driven by functional microorganisms that significantly influence its fate, and these mechanisms include genes, enzyme catalysis and reactive oxygen species (ROS) (Li et al., 2021; Zhang et al., 2022). How-

* Corresponding author.
E-mail: zhangcl@gxu.edu.cn (C. Zhang).

https://doi.org/10.1016/j.jes.2023.09.013
1001-0742/

ever, the current limited understanding of oxidation biologically driven by Sb(III) may be attributed to challenges in the excavation of oxidizing microorganisms and their mechanism. The oxidation genes (i.e., *aioAB, anoA*) and functional proteins (i.e., AioA, AnoA) have been studied (Ye et al., 2022; Zhang et al., 2021a), there is scarce detailed information on extracellular metabolites and their oxidization.

Endogenous humic-like acids (HA) in extracellular metabolites are natural active centers of metalloid redox, and their activity is directly related to HA, especially low molecular weight HA (Zhang et al., 2021b; Zhou et al., 2020). HA is ubiquitous and can transfer accepted electrons to metal ions and organic compounds (Valenzuela et al., 2019; Verbeeck et al., 2020). Quinones were revealed as the main electron accepting moieties in HA. Anthraquinone-2,6-disulfonate (AQDS) is a model compound of HA, and the reduced ($AQDS^{3-\bullet}$, pH > 3.2) and oxidized ($AQDS^{2-}$) forms of AQDS mediate redox by electron transport (Jiang et al., 2009). For example, quinone compounds, as electron transfer in endogenous HA, promote denitrification by *Comamonas* sp. YSF15 (Zhang et al., 2021b), and the low molecular weight (< 3 kDa) fraction of HA was the best promoter due to its more stable redox potential and electron transport activity.

Although the importance of redox mediated by the electron transfer function of quinones has been demonstrated, quantitative charge transfer fluxes have found that quinones could account for only a tiny part of the observed moles of electrons transferred between HA and oxidant (Aeschbacher et al., 2010; Struyk and Sposito, 2001). A positive correlation between oxidation capacity and stable reactive oxygen free radicals in the phenolic components of HA was found [i.e., phenolic hydroxyl (-OH) (Struyk and Sposito, 2001)]. The fate of metalloids is dictated by reactive free radical-induced generation from phenolic acids. Activating phenolic -OH and stabilizing $SQ^{-\bullet}$ can mediate metalloid redox transformation, i.e., As (Qin et al., 2016a). Phenolic is a crucial component of HA, which promotes $SQ^{-\bullet}$ and ·OH formation and then induces the generation of H_2O_2 in an O_2 atmosphere (Qin et al., 2016b; Zhang et al., 2022). Interestingly, the intermediates including $SQ^{-\bullet}$, also play a role in the oxidation process. However, quantitative analysis of intermediate products and electron paramagnetic resonance (EPR) characterization showed that oxidation of phenolic mainly was achieved through the generation of H_2O_2 (oxidation contribution more than 70%), while the free radical contribution was less than 30% (Qin et al., 2016a). These active substances are important in degrading organic pollutants and immobilizing metal ions (Liang and Hu, 2021). These results show that oxidation could be driven cooperatively by electron transfer and ROS.

Extracellular metabolites from *Kaerogenes aerogenes* HC10 were confirmed to be the key fraction to drive Sb(III) oxidation (Rong et al., 2022). In addition, representative phenolic compounds were detected in metabolism using mass spectrometry (Appendix A Fig. S1). These results imply that quinones and phenolic compounds are the best potential promoters for Sb(III) oxidation in extracellular metabolites of *K. aerogenes* HC10. Therefore, chemically defined compounds AQDS and HYD were used as model compounds for quinoid moieties and phenolic compounds in metabolites to explore the oxidation mechanism of Sb(III) (Scheme 1). The objectives of this study were (1) to study the oxidation and kinetics of Sb(III) in extracellular metabolites and explore the Sb(III) oxidation mechanism by H_2O_2 and free radicals with chemical quantitative and EPR characterization and (2) to explore the effect of electron inhibitors and exogenous AQDS on oxidation and elucidate electron transfer mechanisms by electrochemistry characterization.

1. Materials and methods

1.1. Characterization of Sb(III) oxides

K. aerogenes HC10 suspensions (OD600 1.0) were inoculated in LB medium and grown aerobically at 150 r/min at 35 ± 0.1°C in the dark and reached an exponential phase (6 hr), initial stationary phase (24 hr) and initial decline phase (48 hr) (Appendix A Fig. S2). These stages reflected a different accumulation of active components in metabolites. The microflora inoculum was centrifuged at 8000 ×*g* for 10 min, and the supernatant (cell-free filtrate) was collected. Subsequently, the cell-free filtrate was treated with 0.05 mmol/L Sb(III) ($C_8H_4K_2O_{12}Sb_2{\cdot}3H_2O$) and further incubated aerobically at 35 ± 0.1°C for 0, 0.5, 2, 6, 12 and 24 hr. At a predetermined time, 2.0 mL of solution was collected with a syringe from each reactor, and oxidation was immediately stopped by adding 0.1 mL of 6.0 mol/L HCl (Wu et al., 2019a). Samples were filtered through 0.22 μm membrane filters for Sb(III) and total Sb measurements.

1.2. Sb(III) oxidation mechanism mediated by ROS

The chemical structure characteristics of phenolic compounds in metabolites have been confirmed by mass analyze (Appendix A Fig. S1). Therefore, HYD (98%, Macklin, China) was used as a model phenolic compound to investigate the mechanism of Sb species transformation driven by reactive oxygen species (Wu et al., 2019a). To better observe the oxidation caused by extracellular metabolite accumulation, the cell-free filtrate collected at 48 hr were treated with 0.05 mmol/L HYD and 0.05 mmol/L Sb(III). To quantify the contribution of oxygen-induced free radical generation oxidation, cell free filtrate was purged with N_2 for more than 1 hr to remove oxygen (Qin et al., 2016a). To verify the importance of ·OH in the cell-free filtrate, the filtrate was purified with methanol (MeOH, V/V, 2% dosage could scavenge 99% of ·OH) before being used (Qin et al., 2016a). In addition, 0.05 mmol/L phosphate buffer solution (PBS, pH adjusted to 8.1 ± 0.1 according to Appendix A Fig. S3) was used as a substitute to eliminate the intrinsic role of metabolites. All treatments were as follows: (1) cell-free filtrate; (2) cell-free filtrate + 0.05 mmol/L HYD; (3) HYD in PBS; and (4) cell-free filtrate purged with N_2 (N_2 purging) and MeOH (MeOH purging). All treatments were performed in triplicate and cultivated aerobically at 35 ± 1°C for 0, 5, 10, 30, 60, 90 and 120 min. At a predetermined time, the solution was collected to determine pH and quantify Sb(III). The kinetic calculation was carried out to obtain the required kinetic data.

The oxidation mechanism was studied based on the above treatments. The cell-free filtrate treated with 0.05 mmol/L HYD in the absence of Sb(III) was used to quantify the H_2O_2

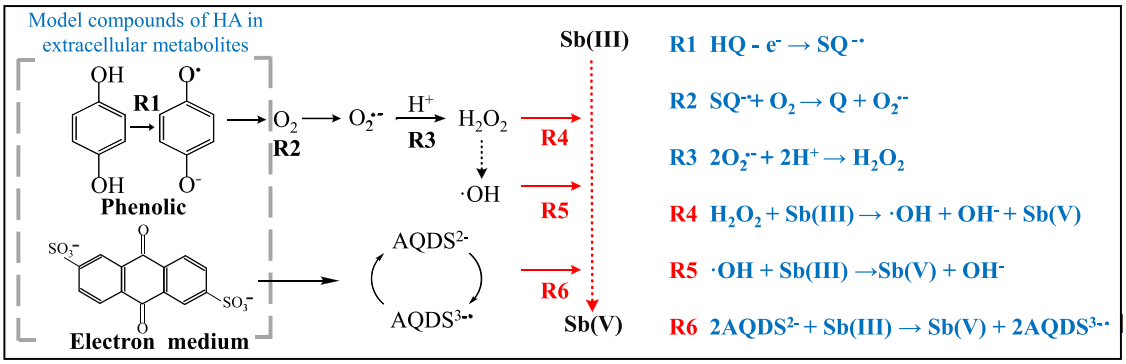

Scheme 1 – Proposed pathways for Sb(III) oxidation mediated by H_2O_2, free radicals and electron transfer in metabolites of *K. aerogenes* HC10.

concentration. The ·OH concentration in the cell-free filtrate and 0.05 mmol/L HYD treatments were quantified. The 10 mL solutions in all treatments were collected at the maximum reaction rate time point (at 60 min, according to the oxidation rate) for free radical (including $SQ^{-\bullet}$, ·OH and $O_2^{\bullet-}$) analysis using electron paramagnetic resonance (EPR). Fluorescence characteristics of low molecular weight compounds in 0.05 mmol/L HYD treatment were characterized by three-dimensional fluorescence characterization (EEM). The solid precipitated mineral residues were collected by freeze-drying from HYD reactors for X-ray photoelectron spectroscopy (XPS), X-ray Diffraction (XRD) and scanning electron microscopy and energy dispersion spectrum (SEM-EDS) characterization.

1.3. *Sb(III) oxidation mechanism mediated by electron transfer*

AQDS (98%, Macklin, China) was used as a model quinone compound to investigate the mechanism of electron transfer (Wu et al., 2020). The cell-free filtrate collected at 48 hr were treated with 0.05 mmol/L /0.5 mmol/L AQDS and 0.05 mmol/L Sb(III). Dicumarol (0.01 mmol/L) was employed as an inhibitor to investigate the oxidation contribution by endogenous electron transfer. A 0.05 mmol/L phosphate buffer solution (PBS, pH = 8.1 ± 0.1) was used as a substitute to eliminate the intrinsic role of metabolites. All treatments were as follows: (1) cell-free filtrate; (2) cell-free filtrate + 0.05 mmol/L /0.5 mmol/L AQDS; (3) cell-free filtrate + dicumarol; and (4) 0.5 mmol/L AQDS in PBS. All treatments were performed in triplicate and cultivated aerobically at 35 ± 1°C for 0, 5, 10, 30, 60, 90, and 120 min. At a predetermined time, the solution was collected, and Sb(III) was quantified. The kinetic calculation was carried out to obtain the required kinetic data.

At the end of incubation, the solutions of all treatments were collected for electrochemical analysis. The solid precipitated mineral residues were collected by freeze drying from AQDS reactors for XPS, XRD and SEM-EDS characterization.

1.4. *Chemical analysis*

Total Sb in solution was prepared using ascorbic acid solution (10%, W/V) and quantified by hydride generation atomic fluorescence spectrometry (HG-AFS, Titan Instruments Co. Ltd., China). An accurate and effective analysis of aqueous Sb(III) concentration with masking agent was performed (Rong et al., 2022). Briefly, an accurate 1.00 mL sample was mixed with 3.0 mL of sodium citrate solution (20 g/L) and 1 mL HCl (50%, V/V) for 30 min and diluted to 10 mL with ultrapure deionized water. Subsequently, the mixture was filtered (0.45 μm) and Sb(III) and total Sb were quantified using HG-AFS. Quality control of Sb species was assessed for each batch sample using labeled recovery. The recoveries of Sb(III) in spiked solution were 98.5%-107.2%.

The H_2O_2 concentration in the cell-free filtrate and 0.05 mmol/L HYD treatments were determined with an assay kit (Nanjing Jiancheng Bioengineering Institute, China). The pH at each time point was measured using a pH meter (S210, Mettler Toledo, Germany). The ·OH concentration was quantified by thiobarbituric acid method (TBA) analysis (Liu et al., 2015; Thomas, 1988).

1.5. *Electrochemical analysis*

The redox potentials were examined by cyclic voltammetry (CV) using an electrochemical workstation (CHI760E, CH Instruments Co., Ltd., Shanghai, China). A saturated calomel electrode was used as a reference, and a platinum electrode was used as the counter electrode (Liu et al., 2020). Carbon cloth (1.5 × 1.5 cm) was used as the working electrode. A 0.2 mL solution was fixed on the carbon cloth using nafion, and PBS (10 mmol/L, pH 7.0) was used as the electrolyte. CV measurements were taken in a potential range of -2.0 to +0.4 V (vs. SCE) with a scan rate of 70 mV/sec. The parameters of CV measurements are listed in support information (Appendix A Table S1).

1.6. *EPR characteristics*

Free radical intermediates including $SQ^{-\bullet}$, ·OH and $O_2^{\bullet-}$ were verified by EPR spectrometry (E500, Bruker, Germany). The $SQ^{-\bullet}$ EPR signals were recorded directly, and 5,5-dimethyl-1-pyrroline oxide (DMPO, ≥97%) and 2,2,6,6-tetramethylpiperidine (TEMP, ≥97%) (0.05 mmol/L) were used as spin trapping agents of ·OH and $O_2^{\bullet-}$, respectively (Qin et al., 2016a; Wu et al., 2019b). The parameters of EPR measurements are listed in Appendix A Table S2.

1.7. *Characterization of precipitates*

Mineral phase samples were analyzed using XRD (Rigaku D/MAX 2500 V, Japan) equipped with Cu-Kα radiation at 40 kV and 40 mA. The scan was 10 to 80° 2θ at 5° 2 θ/min. The XPS signal (Thermo Fisher Scientific, USA) was collected with a monochromatic AI Ka X-ray source. Morphology and elemental composition of mineral phases were determined through electron imaging equipped with SEM-EDS (Phenom Pro 800-07334, Netherlands). Low molecular weight compounds were collected according to previous references (Rong et al., 2022), and then used for EEM analysis (RF-6000, Shimadzu, Japan).

1.8. *Data analysis*

Differences between AQDS and HYD treatments were assessed with the least significant difference test (LSD, $p < 0.05$, IBM SPSS Statistics 22.0). Figures were drawn with Origin Pro 8.0. The response of the solution to Sb(III) oxidation could be quantified with the following equation:

$$\text{Sb(III)ox}(\%) = \left[C_{T-Sb} - C_{Sb(III)}\right]/C_{T-Sb} \times 100\%$$

where Sb(III)ox is the oxidation rate, and $C_{Sb(III)}$ and $C_{T\text{-}Sb}$ are the Sb(III) concentration and total Sb concentration, respectively.

A pseudo-first-order kinetic model was employed to fit the Sb(III) oxidation.

$$\ln(C_t/C_0) = -k_{obs} \cdot t$$

where t (min) is the reaction time, C_t (mmol/L) is the concentration of Sb(III), C_0 refers to the initial concentration of Sb(III), which is 0.05 mmol/L, and k_{obs} is the oxidation rates. The validity of these calculations can be tested using the standard deviation and coefficient of R^2.

2. Results and discussion

2.1. *Characterization of Sb(III) oxides*

The curves in Fig. 1 show the generation of Sb(V) in the cell-free filtrate collected at different times (6, 24 and 48 hr). We found that the oxidation rate constant k_{obs} increased from 0.0073 (6 hr) to 0.0203 (24 hr) and 0.1058 (48 hr) (Appendix A Table S3), suggesting that metabolite oxidants accumulated with an increase in *K. aerogenes* HC10 incubation time, which would induce more Sb(V) generation. This result was confirmed by mass spectrometry, and a significant increase in compound abundance and accumulation of metabolites was observed (Appendix A Fig. S1).

Organic compounds and secondary metabolites, including lipids, sugars, and phenolic compounds, were enriched in the extracellular solution of *K. aerogenes* HC10 (Rong et al., 2022). These self-excreting redox molecules, with oxidizing or transporting electrons, were metabolized by *Klebsiella* sp. and reported in metal ion redox (Wei et al., 2018). A faster oxidation rate was presented at the beginning and then gradually slowed, which may be because oxidants accumulated at the initial stage in metabolites, and were consumed with Sb oxidation.

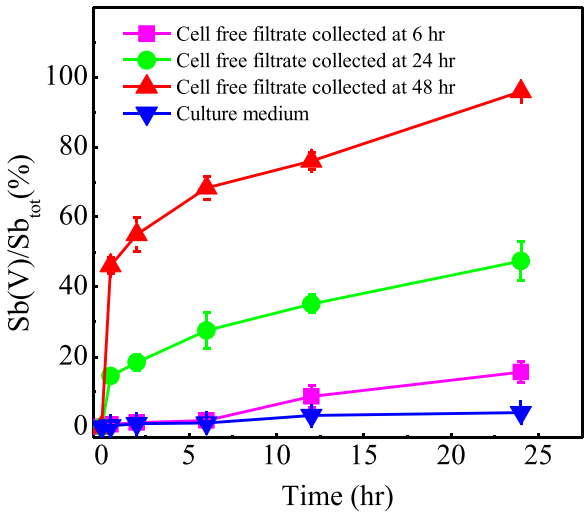

Fig. 1 – The Sb(III) oxidation by cell free filtrate collected at 6 hr, 24 hr and 48 hr incubation time of *K. aerogenes* HC10. Data, means ± SD (n = 3).

2.2. *Sb(III) oxidation mechanisms mediated by reactive oxygen species (ROS)*

2.2.1. *Phenol mediated Sb(III) oxidation and ROS analysis*

Quantifying the acceleration effect of exogenous HYD was used as an effective verification to observe whether exogenous HYD drives Sb oxidation. Cell-free filtrate with 0.05 mmol/L Sb(III) was treated at pH 8.1 ± 0.1 with 0.05 mmol/L HYD in aerobic conditions (Fig. 2**A**). Approximately 20.1 μmol/L (oxidation rate 40.2%) of Sb(V) was accelerated by 0.05 mmol/L HYD treatment during the 120 min (Appendix A Table S4). Fig. 2**B** shows an extremely significantly accelerated oxidation with increasing exogenous HYD. Meanwhile, Sb(III) oxidation profiles were well fit to the pseudo-first-order kinetic model (Appendix A Table S5). The oxidation rate constant of HYD-treated k_{obs} increased from 0.0061 to 0.0276 with 0.05 mmol/L HYD.

Fig. 2**C** plots the H_2O_2 and Sb(V) generation with exogenous HYD treatment in two independent reactors. Exogenous 0.05 mmol/L HYD induced approximately 0.169 (minimum difference value at 10 min) - 0.625 mmol/L (maximum difference value at 90 min) H_2O_2 production, and similar studies were found in a low molecular weight phenolic compound of gallic acid (0.5 mmol/L gallic acid, reaction for 2 hr, pH 9.0) (Wu et al., 2019a, 2019b).

The generated H_2O_2 and the oxidized Sb(III) showed a linear correlation with a correlation coefficient of $r^2 = 0.97$ in 0.05 mmol/L HYD and $r^2 = 0.94$ in the cell free filtrate ($p < 0.01$, Table 1), indicating that Sb(III) oxidation is mainly driven by H_2O_2. H_2O_2 was demonstrated as the main oxidant under alkaline solutions involved in Sb(III) oxidation (Deng et al., 2021), with a pH range of 8.1 to 11.7 (Kong et al., 2015; Leuz et al., 2006), which corresponds to the results of pH 8.1-8.5 in this

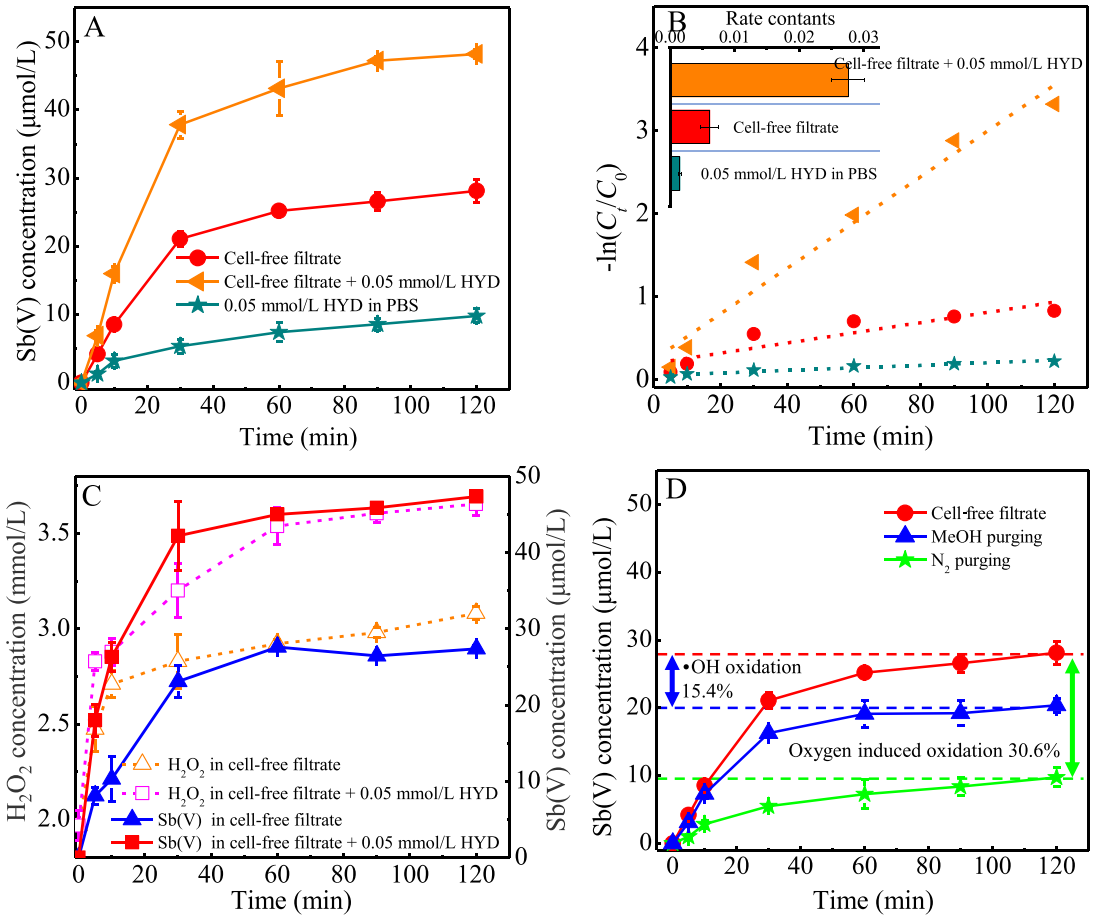

Fig. 2 – Oxidation effects of exogenous 0.05 mmol/L HYD, cell free filtrate and PBS treatments (A) and their kinetic profiles (B); The H_2O_2 and Sb(V) concentration and their correlation (C), Sb(III) Oxidation of cell free filtratemafter purged with N_2 and methanol (MeOH) (D). N_2 was used to purify oxygen from cell free filtrate, before and during incubation. MeOH as ·OH scavenger was added to cell free filtrate before used. Incubation solutions was performed at pH 8.1 ± 0.1, 25 ± 0.1 °C in the dark. Data, means ± SD (n = 3).

Table 1 – Correlation of Sb(V) and H_2O_2 concentration in different treatments.

	H_2O_2 in cell-free filtrate	H_2O_2 in cell-free filtrate + 0.05 mmol/L HYD
Sb(V) in cell-free filtrate	r^2=0.94	–
Sb(V) in cell-free filtrate + 0.05 mmol/L HYD	–	r^2=0.97

study. Electron transfer from reduced HA to O_2 can be a significant source of ·OH at oxic/anoxic interfaces containing organic matter in the dark (Zeng et al., 2020). Specifically, $O_2^{\bullet-}$ in combination with H^+ can produce H_2O_2, and subsequent metal-mediated cleavage to ·OH will further induce the oxidation of Sb. This reaction sequence is called the superoxide-driven Fenton reaction and has been noted in metalloid oxidation (Zhou et al., 2022). TBA results responded to differences in ·OH generation in all treatments. The concentration of ·OH in the 0.05 mmol/L HYD treatment was significantly higher than that in the cell-free filtrate (Appendix A Fig. S4), indicating that Sb(III) oxidation induced the dissociation of H_2O_2 to produce ·OH.

Notably, up to 1.9 mmol/L endogenous H_2O_2 was observed in the cell-free filtrate, explaining the initial inherent oxidation of metabolites (Fig. 2C) and the production of ·OH in cell-free filtrate without HYD treatment (Fig 2C, Scheme 1). Due to the high redox potential of H_2O_2, its reaction rate with Sb(III) is 15.3 $(mol/L)^{-1}\cdot sec^{-1}$, while the ·OH reaction rate is 8.5×10^9 $(mol/L)^{-1}\cdot sec^{-1}$ (Dutta et al., 2005; Lee and Choi, 2002; Pettine et al., 1999). Therefore, as ingredients in Fenton-like reactions, it is reasonable to speculate that H_2O_2 and ·OH could be consumed by Sb(III) in advance (Wu et al., 2019a). References had been proven H_2O_2 is an active component that preferentially drives the oxidation of Sb (Qin et al., 2016a). With the prolongation of time, the decrease in H_2O_2 is another im-

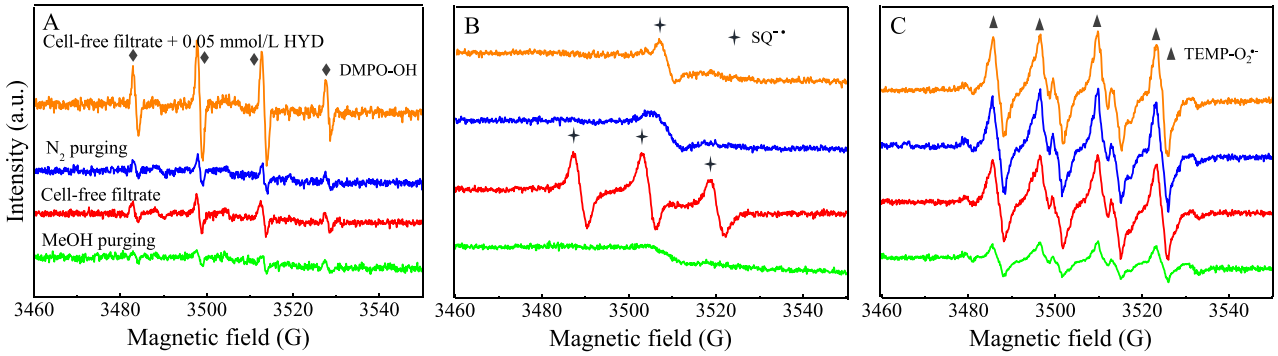

Fig. 3 – EPR spectra of DMPO-OH (A), $SQ^{-\bullet}$ (B) and TEMP- $O_2^{\bullet-}$ (C). DMPO and TEMP were 0.05 mmol/L. pH = 8.3 ± 0.1, T = 25 ± 0.1 °C, incubation time was 60 min.

portant reason for the slow oxidation rate. The oxidation rate was significantly inhibited by MeOH purging at the same incubation time (Fig. 2D). These results suggest that the role of endogenous ·OH in Sb(III) oxidation is indispensable in the current reactor, and its oxidation contribution is 15.4%. The contribution of ·OH approximately 30% of As(III) oxidation in phenolic acid solutions in aerobic conditions by free radical quenching studies has been noted (Qin et al., 2016a). Dissolved organic matter chemical transformation induces ·OH formation (Yang et al., 2022b). As a reactive intermediate, previous studies also revealed that ·OH induced by electrochemical and photocatalytic processes could efficiently oxidize Sb(III) (Jiang et al., 2020). N_2 purification further demonstrates a critical role of O_2 in oxidation induction by free radicals (Fig. 2D), as this process greatly weakens the oxidizing capacity of the cell-free filtrate. A similar phenomenon was observed in organic pollutant degradation by metabolites separated from *Pseudomonas* sp. (Liu et al., 2015), the O_2 atmosphere increased degradation up to 80% and further induced ·OH generation from low molecular weight metabolites. Low molecular weight HA has a more stable redox potential and electron transport activity (Zhang et al., 2021b). Clearly, oxygen-induced oxidation (oxidation rate 30.6% at 120 min) was much stronger than the initial endogenous ·OH in this study. The oxidation was 12.8 μmol/L (or 25.6%) mediated by electron transfer and other oxidants that do not require induction with N_2 purification.

In addition, we observed that the pH was increased in the cell-free filtrate and 0.05 mmol/L HYD treatments (Appendix A Fig. S5), which were responses to HYD induction of the generation of H_2O_2 and subsequent metal-mediated cleavage to OH^- (Scheme 1, R4). In microflora incubation reactors, H^+ can be consumed by $O_2^{\bullet-}$ leading to an increase in pH as well (Zeng et al., 2021b). However, no significant differences of the pH were presented in cell-free filtrate and 0.05 mmol/L HYD treatments, which might be due to form Sb(V)-bearing mineral limitation of the contribution of OH^- in the HYD treatment to the pH increasing (Loni et al., 2020).

2.2.2. *EPR analysis*

Different samples did not present systematic shifts of bands but their intensity changed, which allowed us to infer intermediate moieties involved in Sb oxidation. EPR analysis in the presence of the spin trap DMPO revealed the formation of ·OH (Fig. 3A). The peaks with an intensity ratio of 1:2:2:1 were characteristic DMPO-OH signals, and their peak intensities increased approximately threefold as exogenous 0.05 mmol/L HYD was supplemented. This increasing effect of the signal is explained in terms of the actual formation of ·OH. Similar to other phenolic compounds, HYD quantitatively forms H_2O_2 upon exposure to O_2 and subsequent metal-mediated cleavage to ·OH. Mass spectrometry showed that phenol compounds exist in extracellular metabolites (Appendix A Fig. S1) and can be induced to produce H_2O_2 and hydroxyl radicals, which is the reason the cell-free filtrate without HYD produce·OH. After MeOH purging, no dramatic signal was observed, indicating a quenching effect of ·OH.

$SQ^{-\bullet}$ radicals, as intermediates of the HYD transformation process, further induce ROS generation in solutions containing phenolic compounds according to previous studies (Qin et al., 2016a; Wu et al., 2019b). $SQ^{-\bullet}$ in solution was detected using EPR spectroscopy. Two types of peaks were revealed in the spectrum obtained upon incubation of metabolites with HYD (Fig. 3B): a three-line spectrum (intensity ratio approximately 1:1:1) in the cell-free filtrate treatment corresponding to $SQ^{-\bullet}$ (Eslami et al., 2010; Giulivi et al., 1998) and a one-line signal under the HYD, N_2 and MeOH treatments. Showing exogenous substances changed the contribution of metabolite components to the overall spectrum. HYD, as a strong electron acceptor may change the initial chemical equilibrium of the incubation system and cause the species transformation of $SQ^{-\bullet}$ and the generation of different $SQ^{-\bullet}$ species (Wright et al., 2020). $SQ^{-\bullet}$ induced by phenolics has an obvious characteristic peak between 3480 and 3510, and a single-line peak (pH 10, GA 30 mmol/L) and three-line spectrum (pH 11, 1 mmol/L) were found in the gallic acid response to the differences in electromagnetic signals at different pH values and dosages (Barbehenn et al., 2003; Eslami et al., 2010). Of note, a single peak is much clearer in the mixture containing HYD, while the peak is silent with the addition of MeOH. Additionally, the EEM spectrum of low molecular weight compounds in 0.05 mmol/L HYD showed obvious enhancement (Appendix A Fig. S6). The reduction of quinone to $SQ^{-\bullet}$ after trapping electrons is generally accompanied by increased quinone-like fluorophores and intensity of the π-π^* transitions, especially in the visible range (Cory and McKnight, 2005). This shift explains the darker or more intense fluorescent sig-

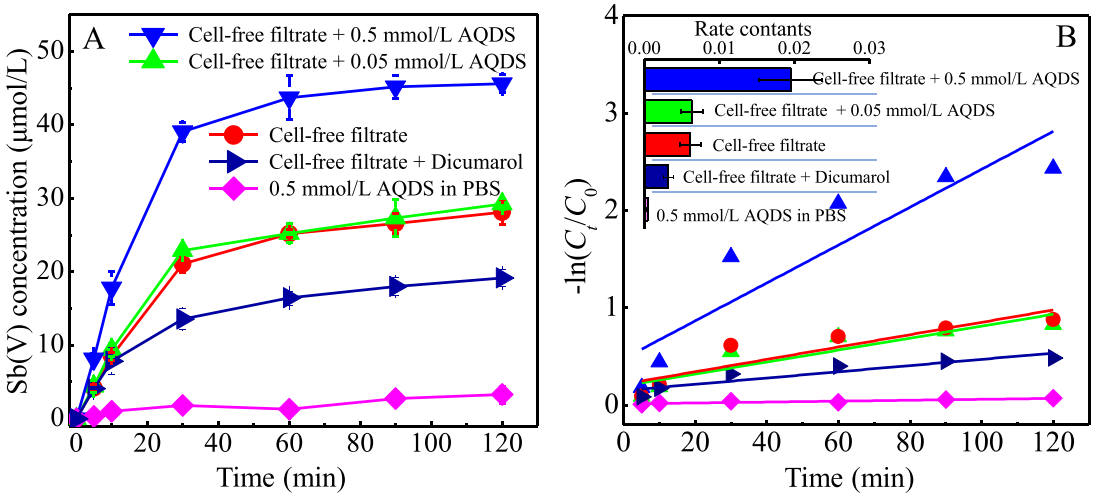

Fig. 4 – Oxidation effects with exogenous 0.05 mmol/L and 0.5 mmol/L AQDS (A) on cell free filtrate (or 0.05 mmol/L PBS) and their kinetic profiles (B). Incubation solutions was performed at pH 8.1 ± 0.1, 25 ± 0.1 °C in the dark. Data, means ± SD (n = 3).

nal of reduced quinones. This result indicates that $SQ^{-\bullet}$ participates in Sb(III) oxidation, which were responses to Sb(III) oxidation mediated by HYD redox products.

As a moderately reactive intermediate and a transient group, the steady state of $O_2^{\bullet-}$ would be no more than 0.1 nmol/L even in the presence of a high concentration superoxide dismutase, so the effect of $O_2^{\bullet-}$ is negligible (Wu et al., 2019b). The peak intensity of $O_2^{\bullet-}$ increased slightly with the addition of HYD (Fig. 3C). The oxidation capacity of the cell-free filtrate was reduced after N_2 purification. Notable, the $O_2^{\bullet-}$ formation was not dramatically inhibited after N_2 purification, which may be due to a trace of unremoved O_2 in solution. Dissolved Humics can be induced to produce a large number of reactive oxygen species in a low concentration oxygen atmosphere, and lower molecular weight dissolved humic generated more $O_2^{\bullet-}$ (Zeng et al., 2021a). The extracellular metabolites of strain HC10 contain a large amount of active phenolic compounds, which may be reason the $O_2^{\bullet-}$ in cell-free filtrate did not significantly reduce after N_2 purging.

2.3. *Sb(III) oxidation mediated by electron transfer*

2.3.1. *AQDS mediated Sb(III) oxidation*

Cell-free filtrate solutions with 0.05 mmol/L Sb(III) were treated at pH 8.1 ± 0.1 with 0.05 mmol/L/0.5 mmol/L AQDS in aerobic conditions (Fig. 4A). Approximately 18.0 μmol/L (oxidation rate 36.0%) of Sb(V) was accelerated by 0.5 mmol/L AQDS treatment at 30 min, while the role of 0.05 mmol/L AQDS was inconspicuous (Fig. 4B). HA bound to Sb(III) species might be involved in the oxidation process because the electron-acquiring ligand center of HA may be activated (Quentel et al., 2004). These ligands, as important components of HA, are closely related to electron transfer and promote the redox of metalloids by electron acceptance and release based on quinone structure. The data also showed oxidation capacity in N_2 purging (Fig. 2D), indicating that quinones were the drivers of the oxidation factor in an oxygen shielding atmosphere. Electron inhibition also confirmed the effect of quinones on oxidation through electron transfer (Fig. 4). Sb(III) oxidation profiles were well fit to the pseudo-first-order kinetic model. Fig. 4B and Appendix A Table S8 show that the oxidation rate constant gradually increased from 0.0061 (cell free filtrate) to 0.0195 (0.5 mmol/L AQDS) when the initial pH was 8.1 ± 0.1. However, the oxidation was limited after 30 min. In complex systems containing different species of quinones and a mixture of Sb(III) and Sb(V) the extent of Sb(III) oxidation will depend on the geochemical parameters, e.g., the ratios of Sb(V)/Sb(III) as well as of quinone/reduced quinones (Jiang et al., 2009; Yang et al., 2022a). In addition, as mentioned above, other redox activity ligands in metabolites may also induce reduction reactions (Min et al., 2022). Oxidation almost disappeared in the defined reaction system of PBS (pH 8.1 ± 0.1) with exogenous 0.5 mmol/L AQDS, indicating the existence of electron acceptors in metabolites to accept electrons transferred from AQDS. Mass spectrometry analysis combined with previous analyses implicated some organic acid compounds (i.e., macrocyclic compounds) and disulfide detected in metabolites (Appendix A Fig. S1) as electron acceptors to receive electrons from AQDS during the Sb(III) oxidation process (Min et al., 2022). Notably, 0.5 mmol/L HYD treated in PBS still exhibited a good oxidation capacity (Fig. 2A), indicating that different mechanisms between HYD and AQDS mediate Sb(III) oxidation and need to be further explored.

2.3.2. *Electrochemical analysis*

Quinone, as a redox-active functional moiety of HA, mediates the oxidation of Sb. CV scanning showed the presence of one obvious reduction peak (potentials of -0.5 ~ -0.6 V) and one slight oxidation peak (potentials of -0.1 V), indicating a stronger oxidation capacity (Fig. 5B). A weak redox couple peak exists in the metabolite response to the presence of endogenous electron transfer (Li et al., 2013; Xia et al., 2010). The potentials of the peak in PBS with 0.05 mmol/L AQDS treat-

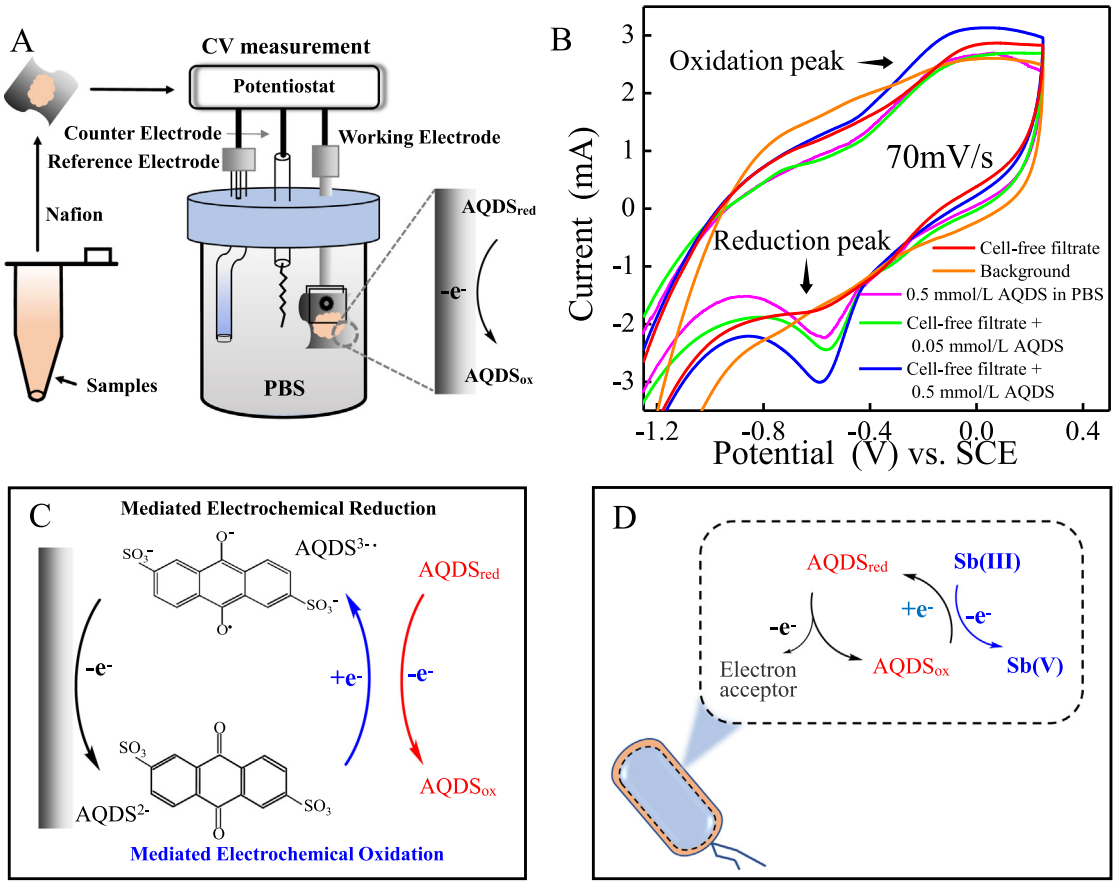

Fig. 5 – Cyclic voltammetry (CV) test device and procedure (A); Cyclic voltammetry curve of reaction solution in cell free filtrate and its improvement program by AQDS (B); Schematic diagram of electron transport on working electrode (C); Sb(III) oxidation was mediated by AQDS (D). The electrochemical cell consists of carbon cloth (1.5 x 1.5 cm) as working electrode, AgCl solution as reference electrode and platinum wire as counter. Samples were fixed on carbon cloth using Nafion binder, and signals were collected in electrolytic cell. The "background" was a carbon cloth only.

ment were consistent with those of the cell-free filtrate, indicating that endogenous electron transfers were AQDS or compounds with similar structures. This result was in response to AQDS as an electron center of metabolites mediating the oxidation of Sb(III). The $AQDS^{2-}$ - $AQDS^{3-\bullet}$ redox couple has long been considered an electron-transfer mediator, and $AQDS^{2-}$ can act as an electron acceptor-mediated oxidation of metals (Lan et al., 2019). As a typical electron transfer regulatory pump, the composition of quinones and their participation in redox are controlled by *arcB-arcA* genes in cells (Franza and Gaudu, 2022). Functional annotation of the draft genes showed that the *arcA* and *arcB* genes were identified in *K. aerogenes* HC10 (Appendix A Table S9), which were the basis of quinone production and electron transfer. A previous study showed that *Klebsiella* sp. can produce quinone compounds (2, 6-di-tert-butylbenzoquinone) as an electron transfer and mediate electron transport directly (Guo et al., 2020; Niu et al., 2020). Although the CV signal was enhanced by supplementation with AQDS, no significant acceleration of oxidation was observed in the 0.05 mmol/L AQDS treated group (Fig. 4A), responding to the weakening effect of H_2O_2 and ·OH as stronger oxidants. However, the CV peak intensity significantly increased with the acceleration of Sb(III) oxidation under 0.5 mmol/L AQDS treatment, indicating that stronger electron transfer could accelerate the oxidation.

Therefore, a potential oxidation mechanism of Sb in metabolites mediated by electron transfer was proposed: Quinones in metabolites could acquire electrons from Sb(III) and transfer electrons to electron acceptors. In this process, Sb was oxidized, while quinone reduction-oxidation alternated. Therefore, quinone acts as an electron relay station to accelerate the oxidation of Sb (Fig. 5D).

2.4. *Oxidation product analysis*

The XPS results provided direct evidence of Sb oxidation. The peaks at binding energies of 539.9 and 539.1 eV corresponded to Sb(V) (7.46%) and Sb(III) (92.54%) (Appendix A Table S10) (Li et al., 2022), indicating that Sb(III) was the dominant species in the PBS treatment. Subsequently, a new $Sb3d_{3/2}$ peak appeared at 531.1 eV and was assigned to the Sb(V) peaks under the AQDS and HYD treatments (Fig. 6B), indicating the redistribution effect of Sb species (Rong et al., 2022). The XRD characteristic peak mainly corresponds to the composition of Sb(V)-bearing mineral mopungite [$NaSb(OH)_6$] and Sb(III) mineral senarmontite (Sb_2O_3) (Fig. 6C) (Loni et al., 2020). The remainder

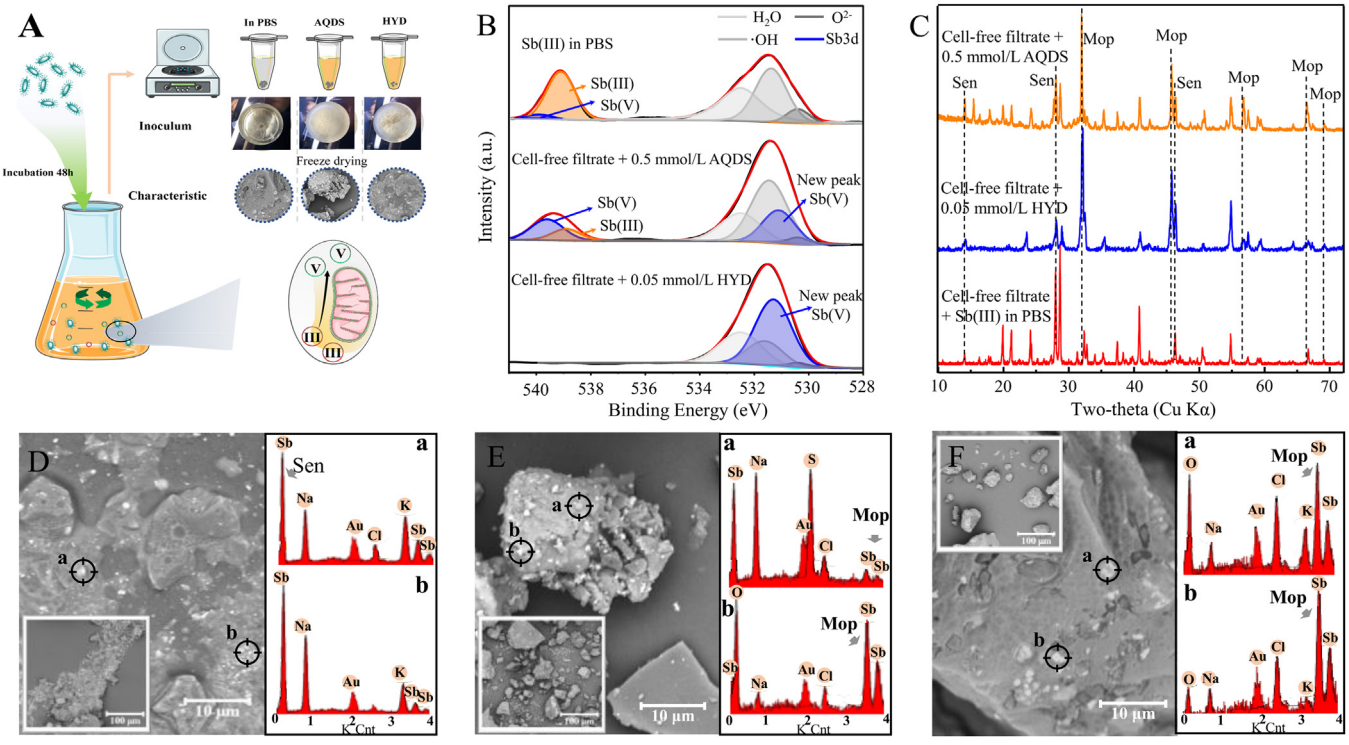

Fig. 6 – Collected procedures of solid precipitates (A); Characterization of solid precipitates collected from the Sb(III) in PBS, AQDS and HYD groups: XPS spectra of Sb3d (B), XRD patterns (C), and SEM-EDS images of Sb(III) in PBS (D), 0.5 mmol/L AQDS treatment (E) and 0.05 mmol/L HYD treatment (F). Sen: senarmontite (Sb_2O_3), Mop: mopungite [$NaSb(OH)_6$].

precipitates (other peaks) were composed of Na^+, K^+ and another mineral ion, which were retained in solids as subsidiary components and confirmed by SEM-EDS (Fig. 6D, E, F). Grayish mineral particles were formed on the solid surface of the HYD and AQDS treatments, in striking contrast with no oxidation in PBS after incubation at 120 min. The strongest peak of Sb in the PBS-treated reactor appeared on the left side of the bands, while the peak shifted to right after the AQDS and HYD treatments, which supports the Sb(III) oxidation and formation of secondary Sb(V)-bearing minerals (Loni et al., 2020). Notably, OH^- was consumed by the generation of Sb(V)-bearing minerals, which may be the reason there was no significant difference in pH in the HYD/AQDS and cell free filtrate treatments (Appendix A Fig. S5). Weak Sb(V)-bearing mineral characteristic peaks were observed in PBS that lacked AQDS or HYD amendment, responding to weak oxidation induced by dissolved oxygen or photocatalysis in solution (Jiang et al., 2020).

2.5. *Environmental significance*

Sb contamination in soil is likely to continue garnering environmental concern because Sb is being fed into soil by the mining industry and a diverse array of other industries. Although Sb(III) is more prevalent in anaerobic paddy soil or sediments (Johnston et al., 2020; Kong et al., 2021), the Sb(III) content was 588.12 mg/kg (accounting for 40.7% of the total Sb) in aerobic soils (Qun et al., 2022). In fact, high concentrations of Sb(III) are generally detected under aerobic conditions, with easier mobility and eventual uptake by crops. This study complements and validates recent reports that *K. aerogenes* HC10 may initiate biologically driven oxidation in Sb-contaminated environments and is induced to form Sb(V)-bearing minerals with mineral ions (i.e., K^+, Na^+) for immobilization. This work process led to a deeper understanding of Sb environmental behavior as well as its precipitation and sequestration in the form of secondary minerals. In previous studies, the oxidation characteristics of independent cell and extracellular metabolites had been demonstrated (Rong et al., 2022), and the metabolite-driven oxidation is much higher than cell-driven oxidation. This study emphasizes the oxidation mechanism of extracellular metabolites, and their role in accelerating Sb(III) oxidation in soils should not be overlooked given their abundance, ubiquity, and mobility., Therefore, rapid oxidation and retention of metalloids can be achieved by using a very small amount of exogenous electron transfer or oxidization-inducing substances. This study highlights the importance of functional microbial metabolites in the environmental behavior of toxic metalloids.

3. Conclusions

We herein propose the mechanism of extracellular oxidation of Sb(III) by *K. aerogenes* HC10. Supplementation with exogenous HYD and AQDS significantly accelerated the oxidation of metabolites. As important active components of metabolites, phenolic acids could subsequently mediate the formation of H_2O_2 for Sb(III) oxidation. In addition, $SQ^{-\bullet}$ participates in oxidation, and H_2O_2 and ·OH were the main oxidants responsi-

ble for Sb(III) oxidation. The EPR characteristics showed that ·OH, $SQ^{-\bullet}$ and $O_2^{\bullet-}$ were important intermediates in the oxidation process. Electrochemical analysis showed that quinone as an electron transfer in metabolites mediated Sb(III) oxidation. Sb(V)-bearing mineral mopungite [$NaSb(OH)_6$] formation reduces the mobility of Sb. This study elucidates the mechanism of Sb oxidation mediated by bacteria and offers a novel idea about Sb(V) bioremediation.

Declaration of Competing Interest

The authors declare that they have no known competing financial interests or personal relationships that could have appeared to influence the work reported in this paper.

Acknowledgment

The work was supported by the National Natural Science Foundation of China (No. 42267001), and the College Young and Middle-aged Teachers' Basic Ability Improvement Project of Guangxi, China (No. 2023KY0393).

Appendix A Supplementary data

Supplementary material associated with this article can be found, in the online version, at doi:10.1016/j.jes.2023.09.013.

References

Aeschbacher, M., Sander, M., Schwarzenbach, R.P., 2010. Novel electrochemical approach to assess the redox properties of humic substances. Environ. Sci. Technol. 44, 87–93.

Barbehenn, R.V., Poopat, U., Spencer, B., 2003. Semiquinone and ascorbyl radicals in the gut fluids of caterpillars measured with EPR spectrometry. Insect Biochem. Mol. Biol. 33, 125–130.

Bolan, N., Kumar, M., Singh, E., Kumar, A., Singh, L., Kumar, S., et al., 2022. Antimony contamination and its risk management in complex environmental settings: a review. Environ. Int. 158, 106908.

Cory, R.M., McKnight, D.M., 2005. Fluorescence spectroscopy reveals ubiquitous presence of oxidized and reduced quinones in dissolved organic matter. Environ. Sci. Technol. 39, 8142–8149.

Deng, R., Chen, Y., Deng, X., Huang, Z., Zhou, S., Ren, B., et al., 2021. A critical review of resistance and oxidation mechanisms of Sb-oxidizing bacteria for the bioremediation of Sb(III) pollution. Front. Microbiol. 12, 738596.

Dutta, P.K., Pehkonen, S.O., Sharma, V.K., Ray, A.K., 2005. Photocatalytic oxidation of arsenic(III): evidence of hydroxyl radicals. Environ. Sci. Technol. 39, 1827–1834.

Eslami, A.C., Pasanphan, W., Wagner, B.A., Buettner, G.R., 2010. Free radicals produced by the oxidation of gallic acid: an electron paramagnetic resonance study. Chem. Cent. J. 4, 15.

Franza, T., Gaudu, P., 2022. Quinones: more than electron shuttles. Res. Microbiol. 173, 103953.

Giulivi, C., Forlin, A., Bellin, S., Cadenas, E., 1998. Reactions of halogen-substituted aziridinylbenzoquinones with glutathione - Formation of diglutathionyl conjugates and semiquinones. Chem. Biol. Interact. 108 (3), 137–154.

Guo, Y., Wang, G., Zhang, H., Wen, H., Li, W., 2020. Effects of biofilm transfer and electron mediators transfer on *Klebsiella quasipneumoniae* sp. 203 electricity generation performance in MFCs. Biotechnol. Biofuels 13, 162.

Jiang, J., Bauer, I., Paul, A., Kappler, A., 2009. Arsenic redox changes by microbially and chemically formed semiquinone radicals and hydroquinones in a humic substance model quinone. Environ. Sci. Technol. 43 (10), 3639–3645.

Jiang, W., Liu, Y., Liu, F., Li, F., Shen, C., Yang, B., et al., 2020. Ultra-fast detoxification of Sb(III) using a flow-through TiO_2-nanotubes-array-mesh based photoelectrochemical system. Chem. Eng. J. 387, 124155.

Johnston, S.G., Bennett, W.W., Doriean, N., Hockmann, K., Karimian, N., Burton, E.D., 2020. Antimony and arsenic speciation, redox-cycling and contrasting mobility in a mining-impacted river system. Sci. Total Environ. 710, 136354.

Kong, L., Hu, X., He, M., 2015. Mechanisms of Sb(III) Oxidation by pyrite-induced hydroxyl radicals and hydrogen peroxide. Environ. Sci. Technol. 49 (6), 3499–3505.

Kong, T., Lin, H., Xiao, E., Xiao, T., Gao, P., Li, B., et al., 2021. Investigation of the antimony fractions and indigenous microbiota in aerobic and anaerobic rice paddies. Sci. Total Environ. 771, 145408.

Lan, S., Wang, X., Yang, P., Qin, Z., Zhu, M., Zhang, J., et al., 2019. The catalytic effect of AQDS as an electron shuttle on Mn(II) oxidation to birnessite on ferrihydrite at circumneutral pH. Geochim. Cosmochim. Acta 247 (15), 175–190.

Lee, H., Choi, W., 2002. Photocatalytic oxidation of arsenite in TiO_2 suspension: kinetics and mechanisms. Environ. Sci. Technol. 36 (17), 3872–3878.

Leuz, A.K., Hug, S.J., Wehrli, B., Johnson, C.A., 2006. Iron-mediated oxidation of antimony(III) by oxygen and hydrogen peroxide compared to arsenic(III) oxidation. Environ. Sci. Technol. 40 (8), 2565–2571.

Li, Q., Huang, M., Shu, S., Chen, X., Gao, N., Zhu, Y., 2022. Quinone-mediated Sb removal from sulfate-rich wastewater by anaerobic granular sludge: performance and mechanisms. Sci. Total Environ. 838, 156217.

Li, X., Liu, L., Liu, T., Yuan, T., Zhang, W., Li, F., et al., 2013. Electron transfer capacity dependence of quinone-mediated Fe(III) reduction and current generation by *Klebsiella pneumoniae* L17. Chemosphere 92 (2), 218–224.

Li, Y., Zhang, M., Xu, R., Lin, H., Sun, X., Xu, F., et al., 2021. Arsenic and antimony co-contamination influences on soil microbial community composition and functions: relevance to arsenic resistance and carbon, nitrogen, and sulfur cycling. Environ. Int. 153, 106522.

Liang, D.H., Hu, Y., 2021. Application of a heavy metal-resistant *Achromobacter* sp. for the simultaneous immobilization of cadmium and degradation of sulfamethoxazole from wastewater. J. Hazard. Mater. 402, 124032.

Liu, S., Wang, J., Lyu, H., Liu, G., Fan, Z., Zhou, J., 2015. Degradation of tetrabromobisphenol-A by extracellular isolates of Pseudomonas sp.fz. Chinese. J. Environ. Eng. 9 (4), 1631–1638.

Liu, T., Luo, X., Wu, Y., Reinfelder, J.R., Yuan, X., Li, X., et al., 2020. Extracellular electron shuttling mediated by soluble c-Type cytochromes produced by *Shewanella oneidensis* MR-1. Environ. Sci. Technol. 54 (17), 10577–10587.

Loni, P.C., Wu, M.X.J., Wang, W.Q., Wang, H.M., Ma, L.Y., Liu, C.Y., et al., 2020. Mechanism of microbial dissolution and oxidation of antimony in stibnite under ambient conditions. J. Hazard. Mater. 385, 121561.

Min, D., Cheng, L., Liu, J.Q., Liu, D.F., Li, W.W., Yu, H.Q., 2022. Ligand-Assisted Formation of Soluble Mn(III) and Bixbyite-like Mn_2O_3 by *Shewanella putrefaciens* CN32. Environ. Sci. Technol. 56, 3812–3820.

Niu, Y., Yuan, L., Liu, B., Wang, R., 2020. Comparative study of extracellular electron transfer mechanism mediated by

electron transfer mediators in two strains of electricigenic bacteria. Chin. Environ. Sci. 40 (11), 4911–4918.
Pettine, M., Campanella, L., Millero, F.J., 1999. Arsenite oxidation by H_2O_2 in aqueous solutions. Geochim. Cosmochim. Acta 63 (18), 2727–2735.
Qin, W., Wang, Y., Fang, G., Liu, C., Sui, Y., Zhou, D., 2016a. Oxidation mechanism of As(III) in the presence of polyphenols: new insights into the reactive oxygen species. Chem. Eng. J. 285, 69–76.
Qin, W., Wang, Y., Fang, G., Wu, T., Liu, C., Zhou, D., 2016b. Evidence for the generation of reactive oxygen species from hydroquinone and benzoquinone: roles in arsenite oxidation. Chemosphere 150, 71–78.
Quentel, F., Filella, M., Elleouet, C., Madec, C.L., 2004. Kinetic studies on Sb(III) oxidation by hydrogen peroxide in aqueous solution. Environ. Sci. Technol. 38 (10), 2843–2848.
Qun, R., Nong, X.Y., Zhang, C.L., Zhong, K., Zhao, H., 2022. Immobilization mechanism of antimony by applying zirconium-manganese oxide in soil. Sci. Total Environ. 823, 153435.
Rong, Q., Ling, C., Lu, D., Zhang, C., Zhao, H., Zhong, K., et al., 2022. Sb(III) resistance mechanism and oxidation characteristics of *Klebsiella aerogenes* X. Chemosphere 293, 133453.
Struyk, Z., Sposito, G., 2001. Redox properties of standard humic acids. Geoderma 102 (3-4), 329–346.
Thomas, D.W., 1988. Handbook of Methods for Oxygen Radical Research, 7. CRC Press, Boca Raton 1988.
Valenzuela, E.I., Avendano, K.A., Balagurusamy, N., Arriaga, S., Nieto-Delgado, C., Thalasso, F., et al., 2019. Electron shuttling mediated by humic substances fuels anaerobic methane oxidation and carbon burial in wetland sediments. Sci. Total Environ. 650, 2674–2684.
Verbeeck, M., Thiry, Y., Smolders, E., 2020. Soil organic matter affects arsenic and antimony sorption in anaerobic soils. Environ. Pollut. 257, 113566.
Wei, W., Li, A., Orcid, S.P., Wang, Q., Orcid, L.Z., Yang, J., et al., 2018. Synthesis of core-shell magnetic nano-composite Fe_3O_4@ microbial extracellular polymeric substances for simultaneous redox sorption and recovery of silver ions as silver nanoparticles. ACS Sustain. Chem. Eng. 6 (1), 749–756.
Wright, J.J., Fedor, J.G., Hirst, J., Roessler, M.M., 2020. Using a chimeric respiratory chain and EPR spectroscopy to determine the origin of semiquinone species previously assigned to mitochondrial complex I. BMC Biol 8 (1), 54.
Wu, T.L., Qin, W.X., Alves, M.E., Fang, G.D., Sun, Q., Cui, P.X., et al., 2019a. Mechanisms of Sb(III) oxidation mediated by low molecular weight phenolic acids. Chem. Eng. J. 56, 190–198.
Wu, T.L., Sun, Q., Fang, G.D., Cui, P.X., Liu, C., Alves, M.E., et al., 2019b. Unraveling the effects of gallic acid on Sb(III) adsorption and oxidation on goethite. Chem. Eng. J. 369, 414–421.
Wu, Y., Luo, X., Qin, B., Li, F., Haggblom, M.M., Liu, T., 2020. Enhanced current production by exogenous electron mediators via synergy of promoting biofilm formation and the electron shuttling process. Environ. Sci. Technol. 54 (12), 7217–7225.
Xia, X., Cao, X.X., Liang, P., Huang, X., Yang, S.P., Zhao, G.G., 2010. Electricity generation from glucose by a *Klebsiella* sp in microbial fuel cells. Appl. Microbiol. Biotechnol. 87 (1), 383–390.
Yang, P., Jiang, T., Cong, Z., Liu, G., Guo, Y., Liu, Y., et al., 2022a. Loss and increase of the electron exchange capacity of natural organic matter during its reduction and reoxidation: the role of quinone and nonquinone moieties. Environ. Sci. Technol. 56 (10), 6744–6753.
Yang, Z.Y., Liu, P., Wang, J., Ding, L., Li, L.Q., Jia, H.Z., et al., 2022b. Microplastics-derived dissolved organic matters accelerate photodegradation of sulfamethazine in wastewater ultraviolet disinfection process. Chem. Eng. J., 140301.
Ye, L., Zhong, W., Zhang, M., Jing, C., 2022. New mobilization pathway of antimonite: thiolation and oxidation by dissimilatory metal-reducing bacteria via elemental sulfur respiration. Environ. Sci. Technol. 56 (1), 652–659.
Zeng, Q., Wang, X., Liu, X., Huang, L., Hu, J., Chu, R., Dong, H., et al., 2020. Mutual interactions between reduced Fe-bearing clay minerals and humic acids under dark, oxygenated conditions: hydroxyl radical generation and humic acid transformation. Environ. Sci. Technol. 54 (23), 15013–15023.
Zeng, Y., Fang, G., Fu, Q., Dionysiou, D.D., Wang, X., Gao, J., et al., 2021. Photochemical characterization of paddy water during rice cultivation: formation of reactive intermediates for As(III) oxidation. Water Res 206, 117721.
Zhang, M.M., Li, Z., Hggblom, M., Young, L., Sun, W.M., 2021a. Bacteria responsible for nitrate-dependent antimonite oxidation in antimony-contaminated paddy soil revealed by the combination of DNA-SIP and metagenomics. Soil Biol. Biochem. 156, 108194.
Zhang, S., Su, J., Ali, A., Zheng, Z., Sun, Y., 2021b. Enhanced denitrification performance of strain YSF15 by different molecular weight of humic acid: mechanism based on the biological products and activity. Bioresour. Technol. 325, 124709.
Zhang, Y., O'Loughlin, E.J., Kwon, M.J., 2022. Antimony redox processes in the environment: a critical review of associated oxidants and reductants. J. Hazard. Mater. 431, 128607.
Zhou, S., Gan, M., Wang, X., Zhang, Y., Fang, Y., Gu, G., et al., 2022. ROS formation driven by pyrite-mediated arsenopyrite oxidation and its potential role on arsenic transformation. J. Hazard. Mater. 443, 130151.
Zhou, X.W., Kang, F.X., Qu, X.L., Fu, H.Y., Alvarez, P.J.J., Tao, S., et al., 2020. Role of extracellular polymeric substances in microbial reduction of arsenate to arsenite by escherichia coli and bacillus subtilis. Environ. Sci. Technol. 54 (10), 6185–6193.